ILASS-Americas 22nd Annual Conference on Liquid Atomization and Spray Systems, Cincinnati, OH, May 2010

Empirical and theoretical analysis of the stability of an air-assisted atomising annular liquid sheet

D. Duke*, D. Honnery and J. Soria
Laboratory for Turbulence Research in Aerospace and Combustion (LTRAC)
Dept. Mechanical & Aerospace Engineering
Monash University, Victoria, Australia

Abstract

A novel application of a correlation-based measurement technique combined with high speed magnified imaging is employed to measure the interfacial stability properties of an air-assisted atomising annular liquid sheet without swirl in the near-nozzle region prior to sheet break-up. Comparison between theoretical stability analysis and such empirical data for the atomisation of liquid sheets has been extremely limited due to the challenging complexities of undertaking measurements in the near-nozzle region where the instabilities amplitudes are extremely small. Using this new technique, frequencies and streamwise growth rates of the initial instabilities can be extracted with sufficient precision and accuracy to permit a comparison with stability analysis models. Variations in the stability properties are investigated against variation in the liquid and air-assisted co-flow momentum. It is further demonstrated that within the region of approximately one sheet thickness from the nozzle exit, the growth of the initial instability is approximately linear. A whole volume-of-fluid linear stability analysis, solving the Orr-Sommerfeld equations, is thus undertaken in order to permit comparison with empirical data in the near-nozzle region. Some improved agreement between empirical and theoretical analysis is observed, permitting a more rigorous analysis of the use of stability analysis as an analytic tool for sprays.

*Corresponding Author: daniel.duke@eng.monash.edu.au

1 Background

Considerable effort has been put into the study of the breakup of annular liquid sheets [1, 2, 3] however an understanding of the physics of the breakup process and the effect of input conditions to the behaviour of the breakup has been elusive due to the large range of scales present in the process, and the complex nature of the highly turbulent breakup process.

High speed digital photography allows a more detailed interrogation of the complex processes occurring at very short time scales and small length scales. Furthermore, image correlation methods [4] permit improved quantitative analysis of the spray as compared to line-of-sight measurements [5, 6]. These improved measurements reveal further levels of complexity in the breakup process and highlight some interesting phenomena in the evolution of small instabilities leading to breakup.

Linear stability analysis has long been employed to improve understanding of the growth of instabilities in liquid sheets [7, 8], however limited empirical data has traditionally been available at the near-nozzle region where such tools are useful. In this paper, new correlation measurements of an atomising annular liquid sheet are compared with linear stability analysis to demonstrate regimes under which such analysis may be valid.

2 Methodology

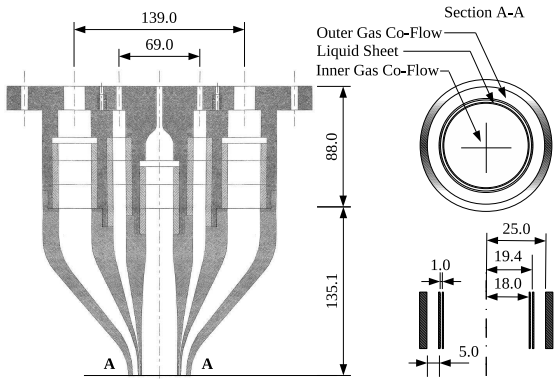

Figure 1. Annular nozzle design.

2.1 Experiment Setup

An annular water sheet of thickness $h = 1$mm and inner radius $r_i = 18.4$mm is exposed to dual co-flowing air streams as per Fig. 1. The gas and liquid flows are purely axial (no swirl). The water is doped with a small concentration of dye to improve contrast, and is recirculated from a reservoir. Compressed air is supplied independently to the inner jet and outer annulus through a series of settling

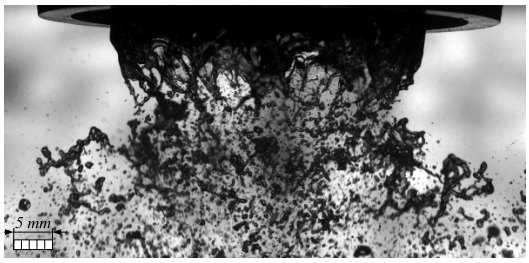

Figure 2. Raw image of spray at $Re_w = 400$, $Re_o = 8900$. Exposure time is $25\mu s$.

screens. Canonical non-dimensional measurement parameters for the annular sheet (see [5, 9, 10]) are the Reynolds Number of the gas and liquid phases, the Weber Number of the liquid sheet and the Momentum Ratio of the gas and liquid phases for each co-flow;

$$\mathrm{Re_{i,o,w}} = \left(\rho \overline{\mathrm{U}} \mathrm{L}/\mu\right)_{\mathrm{i,o,w}}, \tag{1}$$

$$\mathrm{We_w} = \left(\rho \overline{\mathrm{U}}^2 \mathrm{L}/\sigma\right)_{\mathrm{w}}, \tag{2}$$

$$\mathrm{MR_{i,o}} = \left(\rho \overline{\mathrm{U}}^2 \mathrm{A}\right)_{\mathrm{i,o}} / \left(\rho \overline{\mathrm{U}}^2 \mathrm{A}\right)_{\mathrm{w}}, \tag{3}$$

where the subscripts i, o, w represent the inner co-flow jet, outer co-flow and water sheet, the characteristic length scale L is taken as the inner gas co-flow diameter, or the liquid sheet or outer co-flow annulus thickness. The characteristic length scale of sheet displacement is the sheet thickness, $h = 1$mm. The characteristic mean exit velocity $\overline{U}$ is taken as the mass flow rate measured from the supply averaged over the known area of the exit plane of the inner co-flow jet, water sheet or outer co-flow;

$$\overline{U}_{i,o,w} \equiv \left(\dot{m}/(\rho A)\right)_{i,o,w}. \tag{4}$$

Instability velocities on the sheet are non-dimensionalised by the sheet mean velocity $\overline{U}_w$. The instability of the liquid phase undergoing atomisation is non-dimensionally expressed as the Strouhal Number;

$$\mathrm{St} = f_{\mathrm{peak}} \mathrm{L}/\overline{\mathrm{U}}_{\mathrm{w}}. \tag{5}$$

The conditions presented in this paper are shown in Table 1. The motion of the outer surface of the sheet is recorded with a *MotionPro X3* 1.3 Megapixel monochromatic camera at 4096 frames/s. For the magnified images shown in Fig. 13, a parabolic floodlamp is used as a high-intensity light source. For the larger field of view images shown in Fig 12, an LED array has been developed as a large volume light source, with the LEDs pulsed in $25\mu s$

Table 1. Experimental Conditions.

Outer Co-Flow					
Re_w	$\overline{U}_w$ m/s	We_w	Re_o	$\overline{U}_o$ m/s	MR_o
400	0.35	1.71	700	2.19	0.26
400	0.35	1.71	2100	6.55	2.4
400	0.35	1.71	3600	10.98	6.7
400	0.35	1.71	4900	15.29	12.9
400	0.35	1.71	6400	19.70	21.4
400	0.35	1.71	7750	24.03	31.8
400	0.35	1.71	8900	28.07	42.9
400	0.35	1.71	10300	32.43	57.3
2400	2.24	69.82	700	2.19	0.01
2400	2.24	69.82	2100	6.55	0.06
2400	2.24	69.82	3600	10.98	0.16
2400	2.24	69.82	4900	15.29	0.32
2400	2.24	69.82	6400	19.70	0.52
2400	2.24	69.82	7750	24.03	0.78
2400	2.24	69.82	8900	28.07	1.08
2400	2.24	69.82	10300	32.43	1.44
Inner Co-Flow					
Re_w	$\overline{U}_w$ m/s	We_w	Re_i	$\overline{U}_i$ m/s	MR_i
400	0.35	1.71	800	0.35	1
2400	2.24	69.82	5300	2.24	1

bursts in sync with the camera shutter. A 200mm prime lens gives a spatial resolution of 42 pixels per sheet thickness and the total region of interest is 1278×256 pixels or $30 \times 6h$. The camera is capable of recording 3 seconds of continuous footage (12 288 frames), with 6 repetitions per experimental condition.

2.2 Image Processing

The radial velocity of the initial instabilities near the nozzle exit are measured using a correlation image velocimetry technique [4]. The sub-pixel precise radial velocity of the sheet surface is extracted as a function of time and streamwise distance (x) from the nozzle exit. From this data, the power spectrum of the velocity can be determined as a function of x, and the power spectral density can be integrated over x to measure the spatial growth rates of selected instability frequencies. The average image background (without the presence of the liquid sheet) is subtracted from each frame to remove constant features and leave only the contrast difference between the liquid and gas.

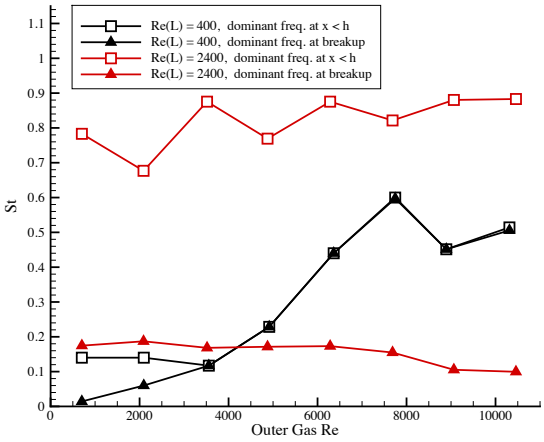

Figure 3. Atomisation Frequency vs outer gas Re. For $Re_w = 400$, the early and breakup instability frequency are similar. For $Re_w = 2400$, the early instability is different to that at breakup.

2.3 Stability Analysis

A linear stability analysis is undertaken to determine the receptivity of the flow at the nozzle exit boundary conditions to instabilities. A whole volume of fluid approach is used [11], where a single set of steady axisymmetric Orr-Sommerfeld Equations are employed with a Chebyshev discretisation to solve the temporal problem for the whole fluid domain. The equations are arranged into a generalised eigenvalue problem;

$$-i\Omega \boldsymbol{A}\hat{\boldsymbol{q}} = \boldsymbol{B}\hat{\boldsymbol{q}}, \text{ where } \hat{\boldsymbol{q}} = [\hat{u}_r \hat{u}_\theta \hat{u}_z \hat{p}]^T , \quad (6)$$

$$\& \ \boldsymbol{q} = \hat{\boldsymbol{q}}(r) \exp\left(i\beta z + i\alpha\theta - i\Omega t\right). \quad (7)$$

For given boundary conditions, the most unstable eigenvalue presents a range of solutions for a range of possible values for complex β. On the complex plane of β, a family of solutions is extracted which have an oscillating and growing spatial instability (positive β) and an oscillating, stable temporal solution (real Ω). In this family of solutions, the modes with the highest spatial growth rates that are representative of physical solutions are expected to be the dominant solutions and may be compared against empirical results.

3 Results

A still image of the sheet breakup is shown in Fig. 2 for $Re_i = 800, Re_o = 8900, Re_w = 400$. The typical stages of breakup are evident; an initial instability forms at the nozzle exit, followed by the breaking of the sheet into ligaments, followed by the rupture of ligaments into droplets. Some small satellite drops are also formed at the breaking point of

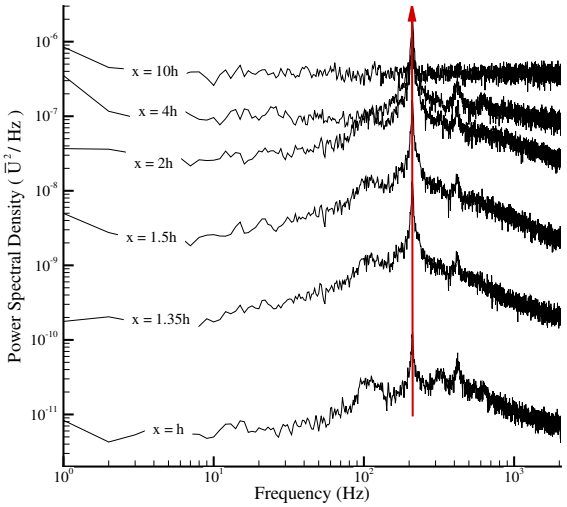

Figure 4. Evolution of Power Spectra for $Re_o = 7750, Re_i = 800, Re_w = 400$. The dominant frequency (red arrow) is consistent to the point of breakup.

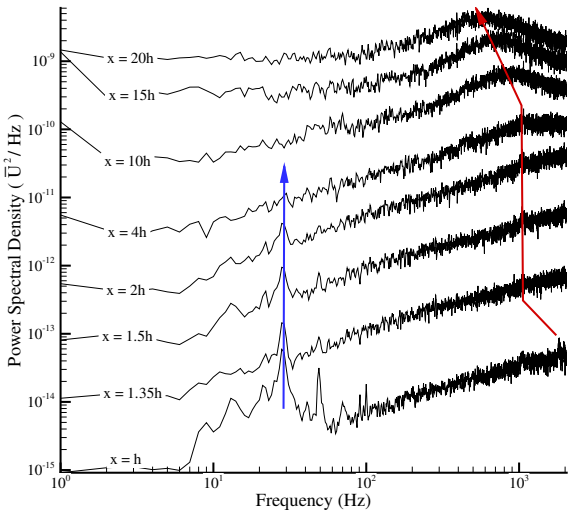

Figure 5. Evolution of Power Spectra for $Re_o = 7750, Re_i = 5300, Re_w = 2400$. The first dominant frequency ranked by energy (red arrow) drops as the breakup point is detected, whereas the second dominant frequency (blue arrow) disappears before the point of breakup. Such behaviour is observed for all gas flow rates studied at higher sheet Re.

the ligaments from the main sheet.

The initial instability is axisymmetric and smooth. The ligament formation process is azimuthally periodic and results in the formation of an arch-shaped edge to the sheet as surface tension forces pinch the edge of the sheet both azimuthally and radially. These regular extrusions are broken off at their ends by the high-speed airflow as they oscillate radially into the high-speed outer gas flow. The extrusions are then refilled with fluid arriving from above. This regular motion originating from the periodic instability waves at the nozzle exit causes waves of ligaments to break off, resulting in waves of droplets.

The azimuthal periodicity of the ligament formation results in an approximately even coverage of the spray. The variation in the size of the ligaments results in greatly varying droplet sizes and velocities. At the breaking point of the ligaments, very small, high-speed satellite drops are observed to be blown away by the high-speed gas flow, whereas at the center of ligaments, larger drops may be formed.

Fig. 12 shows a sequence of one period of the breakup process. The instability waves travel at a notably higher velocity that that of the liquid itself, which has a bulk velocity equivalent to $0.5h$ between each image shown. The radial distribution of droplets is relatively uniform, as the ligaments rotate and shed droplets on both the inward and outward part of the oscillation.

A sequence of the images used in the correlation analysis are shown in Fig. 13, with the camera focused on the tangent edge of the annular sheet's outer surface. A sequence of the same periodic breakup as Fig. 12 is shown, demonstrating the rapid amplification of the instability at a short distance from the nozzle exit.

3.1 Atomisation Frequency

A range of outer gas flow rates at two set liquid sheet conditions $Re_w = 400$ & 2400 with unity inner gas momentum ratio have been studied as per Table 1. Atomisation of the spray onsets at $Re_o > 3500$ for $Re_w = 400$ and $Re_o > 6000$ for $Re_w = 2400$. For most cases where atomisation occurs, at any streamwise distance x between the nozzle exit and point of breakup, a single dominant instability frequency is measured from the average power spectra of 73 728 frames (18 seconds real time).

As per Fig. 3, at low sheet Re, the breakup frequency increases to a point at which a drop is observed. This may be due to separation of the air flow resulting in an uncertain shear velocity. At these conditions, the outer gas momentum has a dominant effect on shear.

At high Re, the outer gas flow has little influence on the breakup process, which indicates that the shear is primarily driven by the liquid momentum. The Momentum Ratios in table 1 are much

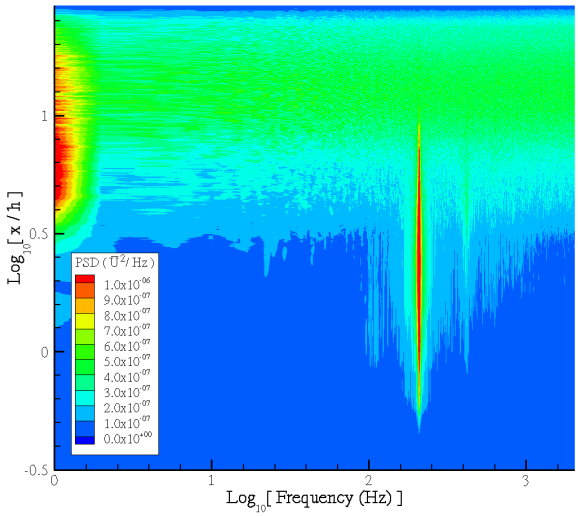

Figure 6. Continuous contours of Power Spectrua for $Re_o = 7750, Re_i = 800, Re_w = 400$. The dominant frequency is consistent to the point of breakup

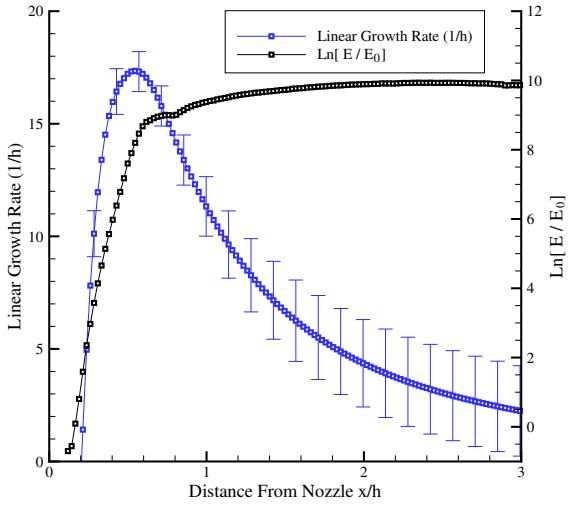

Figure 7. Amplification rates at $Re_w = 400$, $Re_i = 800$, $Re_o = 7700$.

lower at this case, however similarly effective atomisation is observed. The instability at low sheet Re is thus primarily driven by the outer gas flow, and the instability at high sheet Re is primarily driven by the liquid.

Two distinct phenomena are observed in these different regimes. For lower sheet Re, the 'early' instability which dominates near the nozzle exit ($0 < x < h$) is consistently dominant to the point of breakup. For higher sheet Re where the liquid momentum is significant, a dominant high-frequency instability drops in frequency as it approaches breakup, whilst a lower-frequency secondary instability dies out before breakup.

The continuous evolution of the power spectra with (x) at both sheet Re are shown in Figs. 4 and 5. In the low Re case, the dominant frequency is observed from near the nozzle exit to the point of sheet breakup. The continuous contour of power spectral density in Fig. 6 shows this consistency on a linear scale of power spectral density for x. The small waves present at the nozzle exit amplify continuously until each wave results in ligament formation.

In the high Re case (Fig. 5), a much more broadband high frequency instability travels from the nozzle exit to breakup, visible in the high speed images as very small (sub-pixel) high velocity waves. Although this high-frequency peak is not clearly visible in Fig. 5 due to high frequency noise, it contains the majority of the spectral energy spread over a large range. The peak center is indicated in Fig. 3. This higher frequency corresponds to the shedding of the ligaments observed in the high-speed photographs and appears independent of outer gas velocity.

The wavelength approaching breakup is relatively constant, indicating that the drop in frequency may be due to a deceleration of these very high-velocity waves as they grow larger. The process by which some of these waves become ligaments and some do not causes a continuous variation in the shedding frequency, resulting in the broadband noise observed. The low frequency secondary instability is due to a slow flapping of the sheet relative to its ligament shedding frequency. Once the smaller waves amplify enough they dominate the flow and this behaviour is no longer observed. The high noise indicates that a higher temporal resolution is required at high sheet Re, and that the complex instability waveform may not be well-suited to Fourier analysis.

3.2 Evolution of initial instability

The spectral energy at the dominant early instabilities for $Re_o = 7750, Re_i = 8900, Re_w = 400$ & 2400 are shown in Figs. 7 and 8. In all cases a nearly linear growth of the dominant instability is observed near the nozzle exit. The length of this region and the maximum least-squares growth rate are shown vs. outer gas Re in Fig. 9. Linear growth rates are typically 10-20 orders of magnitude per sheet thickness. Based on a previous error analysis [4] and an improved optical setup, instabilities down to $x/h = 0.2$ are observed.

Beyond the linear region, the amount of energy added to the instability before breakup is rela-

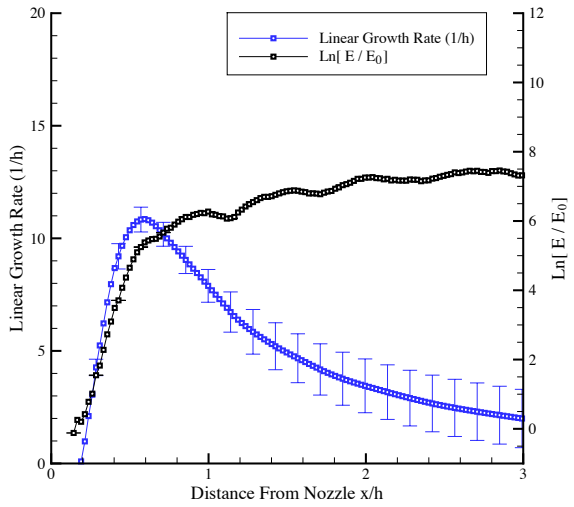

Figure 8. Amplification rates at $Re_w = 2400$, $Re_i = 5300$, $Re_o = 7700$.

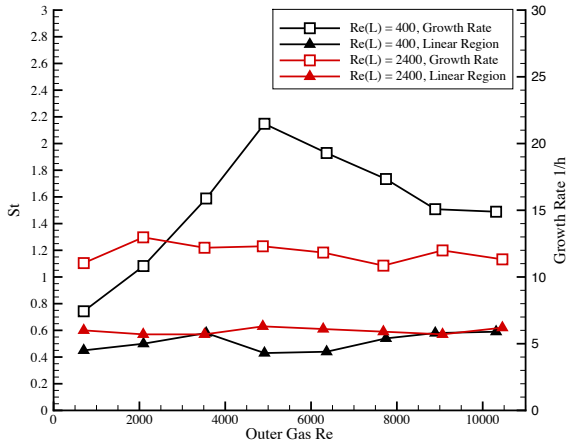

Figure 9. Instability Growth Rates. The length of the linear region is relatively constant. The growth rates for the low Re sheet are affected by the outer gas Re. For the high Re sheet, no variation is observed as the breakup is driven by the liquid momentum.

tively small (one order of magnitude per sheet thickness). The amplification of the spectrum is relatively broadband as shown in Figs. 4, 5 and 6 and is not confined only to the dominant instability. This permits other instabilities which may onset later but grow faster to overtake the previously dominant instability as is observed for the higher sheet Re.

3.3 Stability Analysis

A linear stability analysis has been carried out matching the experimental conditions at $Re_w = 400$. Physical solutions are defined as those which are temporally stable but oscillatory (real Ω) for a certain spatial wavelength and growth rate. The selected solutions from each eigenvalue problem are the leading (most unstable) eigenvalues.

Fig. 10 shows contours of neutral temporal stability (containing physically possible solutions) in complex β space. The maximum growth rates are typically 100-130/h, about 5-6 times larger than observed experimentally, and increase with increasing outer gas flow as expected.

Fig. 11 shows the frequency plane corresponding to the solutions for $Re_o = 700$, with the neutral stability contour indicated. Frequencies at the neutral stability point are typically $St \leq 20$ (up to 7kHz), larger than observed experimentally. The frequency increases with increasing outer gas flow.

4 Discussion and Conclusion

Experimental results indicate that the bulk velocity of the gas flow may not be representative of the shear velocity at the sheet, resulting in a complex relationship between mean flow parameters and breakup properties (frequency & growth rate). For a low Re liquid sheet with high gas momentum ratios, atomisation frequency and growth rate typically increase with outer gas flow Re. For a high Re liquid sheet with low gas momentum ratio, atomisation performance is largely independent of outer gas Re as the liquid momentum drives the instability.

Linear stability analysis predicts sheet amplification rates and instabilities of an order of magnitude larger than observed experimentally, and that for high gas momentum ratios and low sheet Re the growth rate and frequency increase with increasing gas Re.

These preliminary results necessitate further analysis of the gas co-flow in order to more accurately measure the shear velocity at the liquid surface, increased temporal resolution of experimental data, and consideration of alternative diagnostic techniques for the highly resolved velocity data.

5 Acknowledgements

The authors wish to thank Mr. Vassili Kitsios for his advice on the development of the stability analysis, and Mr. Karl Muller for his assistance with the LED lighting system. Mr. Duke was supported by an Australian Postgraduate Award whilst undertaking this research.

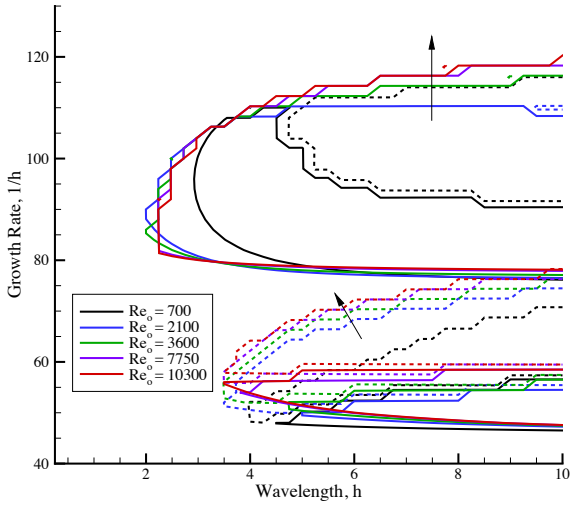

Figure 10. Neutral stability contours matching experimental conditions at $Re_w = 400, Re_i = 800$ for several Re_o as indicated by colour. Arrows indicate trends with increasing outer gas Re.

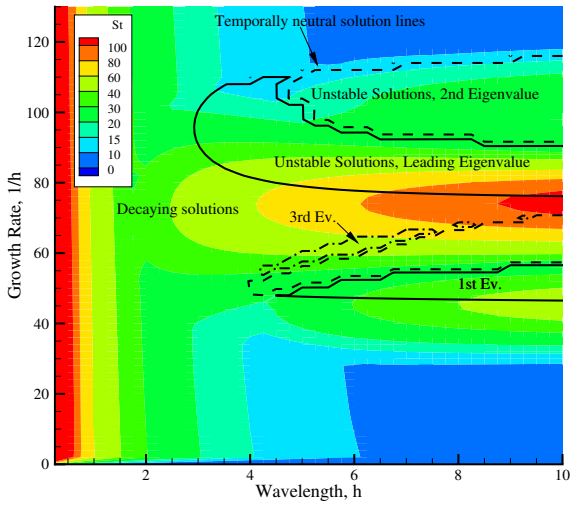

Figure 11. Contours of frequency for stability analysis at $Re_w = 400, Re_i = 800, Re_o = 700$, with neutral stability contours for leading eigenvalues superimposed. Physical solutions lie on the lines of neutral stability.

References

[1] S Kawano, H Hashimoto, H Togari, and A Ihara. *Atomization and Sprays*, 7:359–374, Apr 1997.

[2] G Lavergne, P Trichet, P Hebrard, and Y Biscos. *Journal of Engineering for Gas Turbines and Power*, 115:461–466, Apr 1993.

[3] S Wahono, D Honnery, J Soria, and J Ghojel. *Exp Fluids*, 44(3):451–459, 2008.

[4] D Duke, D Honnery, and J Soria. *Exp Fluids*, 2010. in press. DOI 10.1007/s00348-009-0817-0.

[5] A Lozano, F Barreras, G Hauke, and C Dopazo. *J. Fluid Mech.*, 437:143–173, Jan 2001.

[6] A Mansour and N Chigier. *Physics of Fluids A: Fluid Dynamics*, 3(12):2971–2980, Jan 1991.

[7] S Lin. *Breakup of Liquid Sheets and Jets*. Cambridge University Press, Apr 2003.

[8] J Shen and X Li. *Atomization and Sprays*, 11:491–504, Apr 2001.

[9] I Carvalho and M Heitor. *Exp Fluids*, 24:408–415, Jan 1998.

[10] A Lozano, F Barreras, C Siegler, and D Löw. *Exp Fluids*, 39(1):127–139, Jul 2005.

[11] P Schmid and D Henningson. *Stability and Transition in Shear Flows*. Springer, 2001.

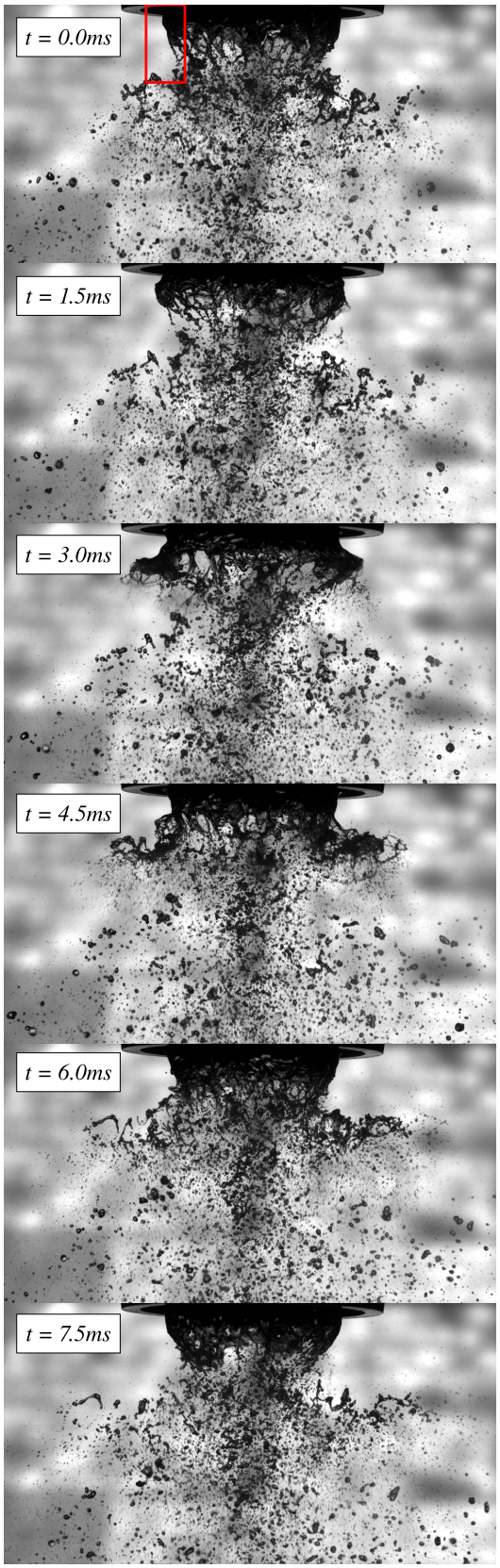

Figure 12. Macro image sequence of spray at $Re_w = 400, Re_o = 8900$. Every third frame is shown at 2000 fps. The red box indicates the region of experimental measurement.

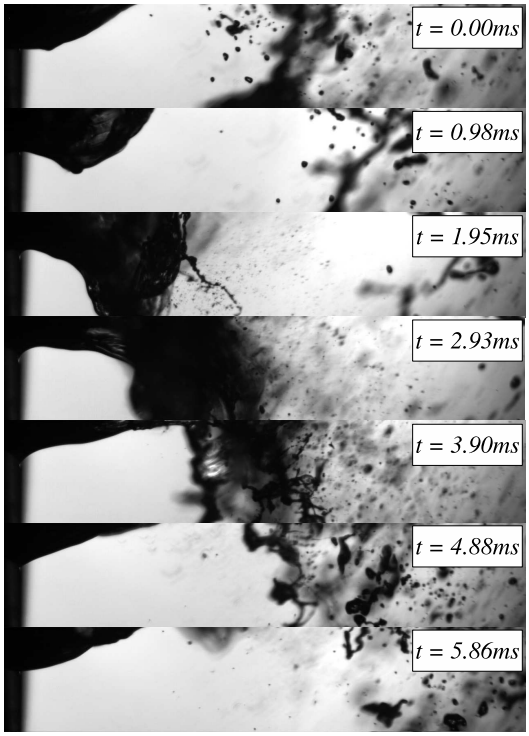

Figure 13. Sample sequence of images used in correlation analysis at $Re_w = 400, Re_o = 8900$. Images are rotated such that the sheet convects left to right. Every fourth frame is shown at 4096 fps. The region of this image relative to the spray is indicated by the red box in Fig. 12.